Detachment-parallel recharge explains high discharge fluxes at the TAG hydrothermal field

Zhikui Guo[1,2], Lars Rüpke[1,*], Sven Petersen[1], Christopher R German[3], Benoit Ildefonse[4], Jörg Hasenclever[5], Jörg Bialas[1], and Chunhui Tao[2,6,*]

[1]GEOMAR Helmholtz Centre for Ocean Research Kiel, Kiel, Germany
[2]Key Laboratory of Submarine Geosciences, SOA, Second Institute of Oceanography, MNR, Hangzhou, China
[3]Woods Hole Oceanographic Institution, Woods Hole, MA, USA
[4]Géosciences Montpellier, University of Montpellier and CNRS, Montpellier, France
[5]Institute of Geophysics, CEN, Hamburg University, Germany
[6]School of Oceanography, Shanghai Jiao Tong University, Shanghai, China
[*]lruepke@geomar.de, taochunhuimail@163.com

S1. Supplementary Figures

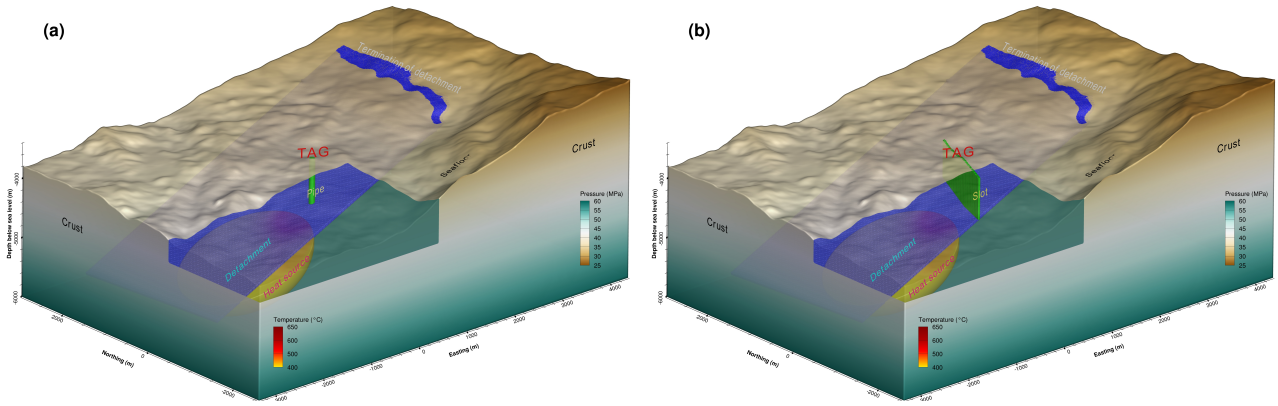

Supplementary Fig. 1: Geometry and pressure initial condition of the novel 3D models. The shallow tectonics as (a) cylindrical shape pipe and (b) slot.

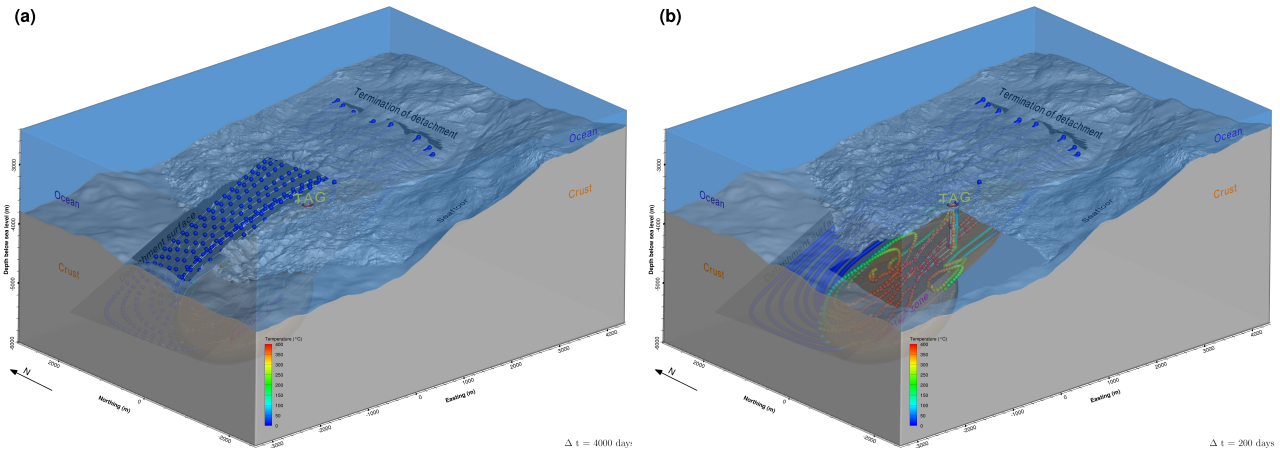

Supplementary Fig. 2: Animation of stream tracers of hydrothermal circulation flow highlighted for (a) recharge flow and (b) discharge flow. These figures are snapshots of the animations, the complete animations can be found at Figshare(doi:10.6084/m9.figshare.16622053).

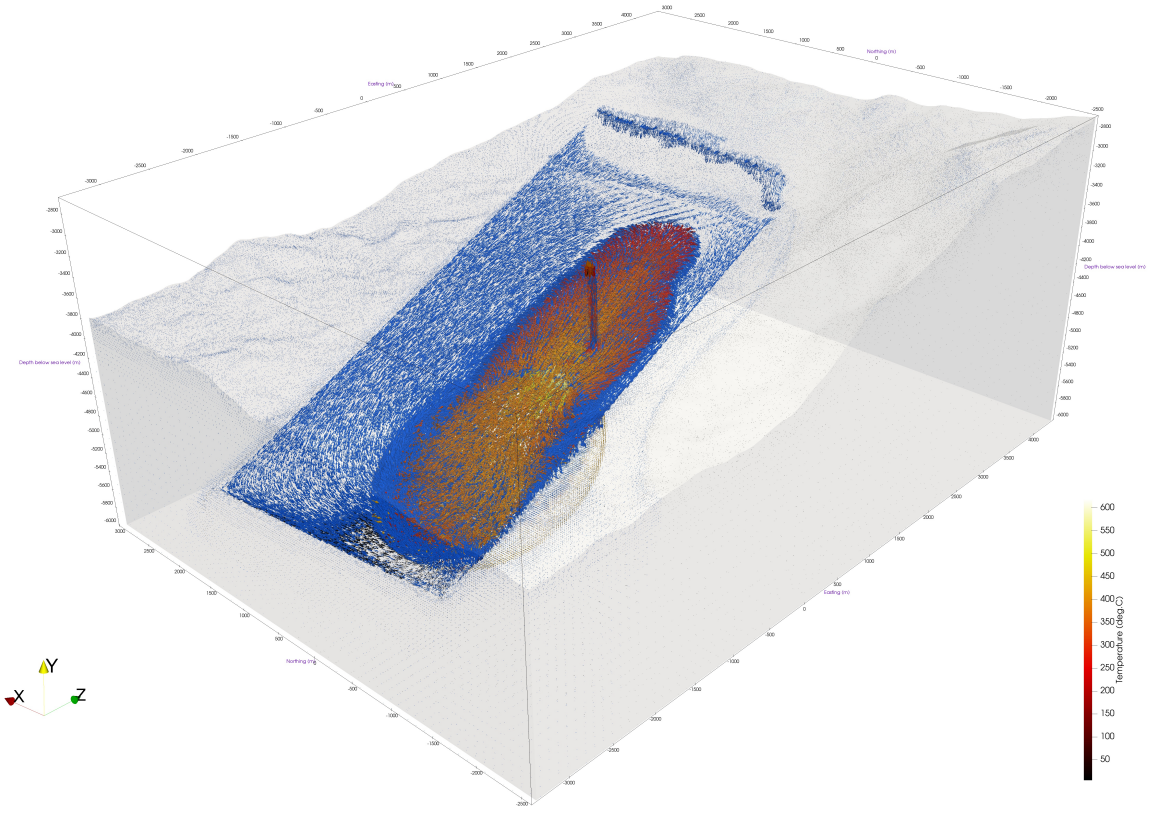

Supplementary Fig. 3: Velocity field distribution in the whole modeling domain. Arrows are scaled by magnitude of fluid velocity ($[log_{10}|\vec{U}|]^{-4}$) and oriented by velocity direction. The velocity arrows are are uniformly sampled from the cells and classified into two kinds. The blue arrows represent recharge flow which is extracted by condition of $U_y < 0$ (negative vertical velocity). The arrows of discharge or up-flow ($U_y < 0$) are color-scaled by fluid temperature. Note that, for visualization reason, the arrows of discharge velocity are shortened approximately 1.35 times with respect to the recharge flow arrows.

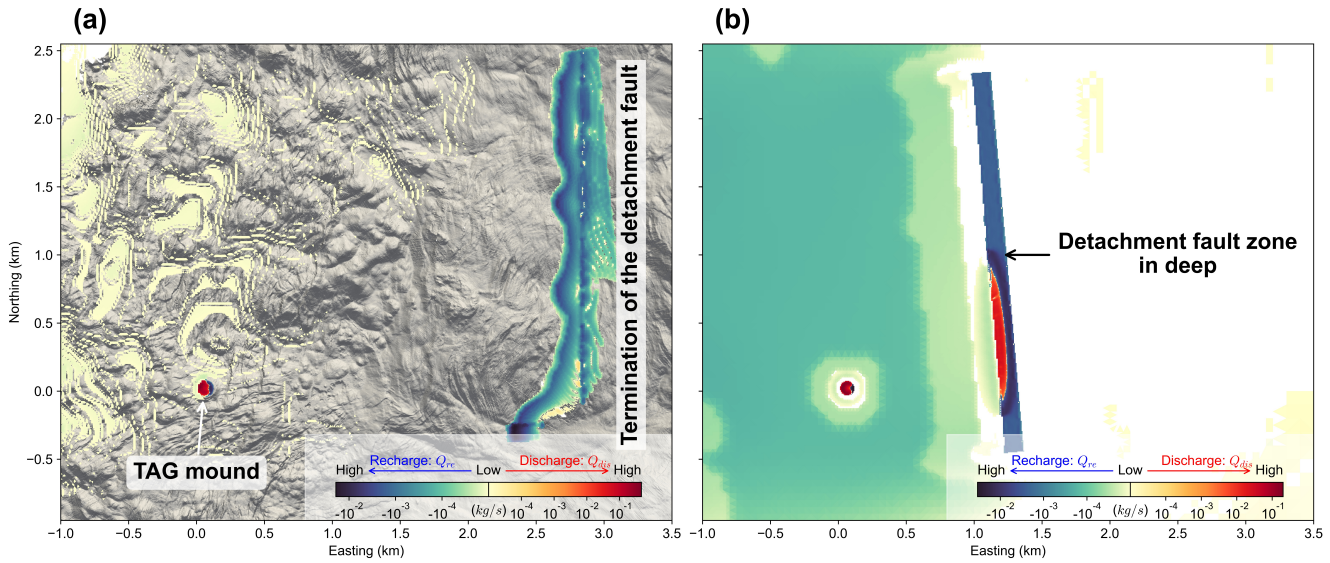

Supplementary Fig. 4: Close up of mass flux distribution on (a) seafloor and (b) horizontal slice at depth of 4km below sea level.

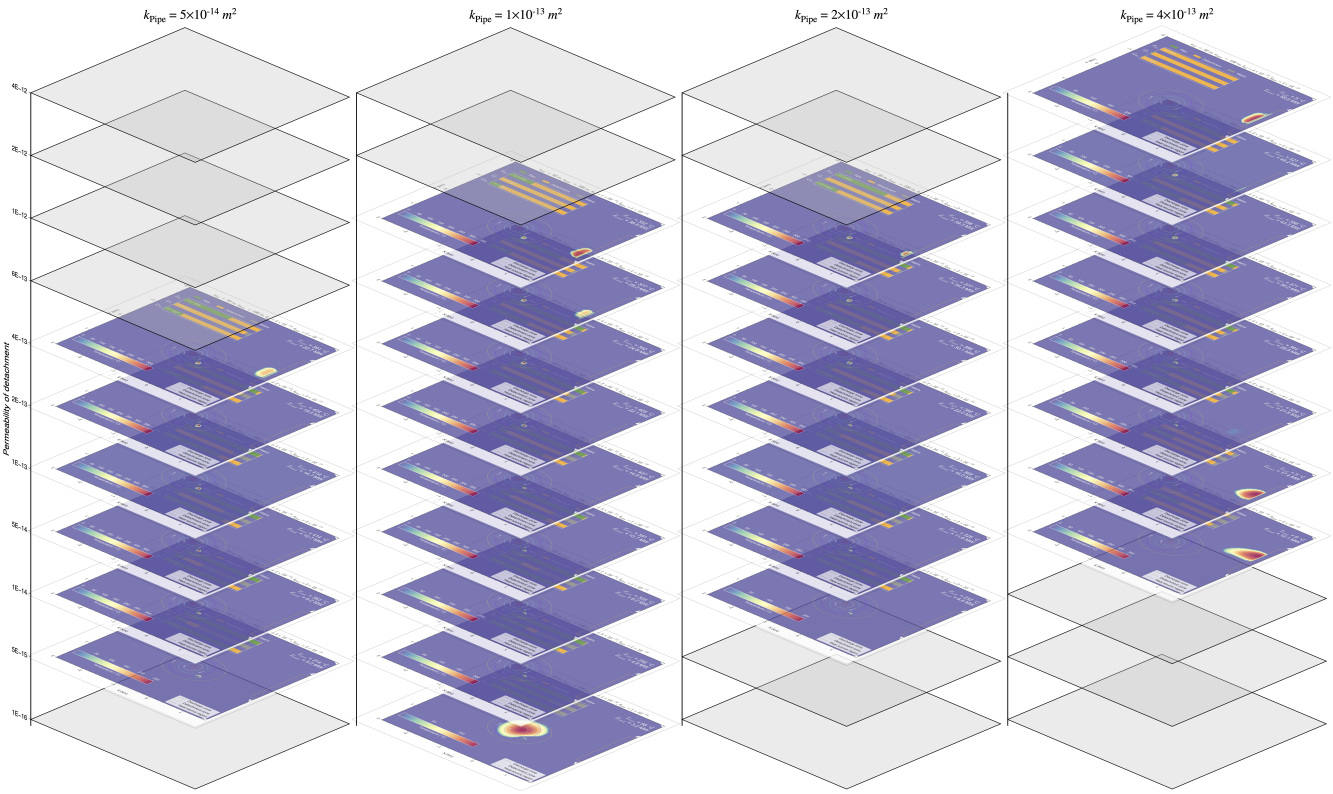

Supplementary Fig. 5: Summary of 3D model (pipe geometry) results at quasi-steady state. Temperature field on seafloor, vent temperature T_{vent}, integrated total discharge mass flow rate Q_{dis} and heat output E_{dis}, conductive heat input E_{cond}

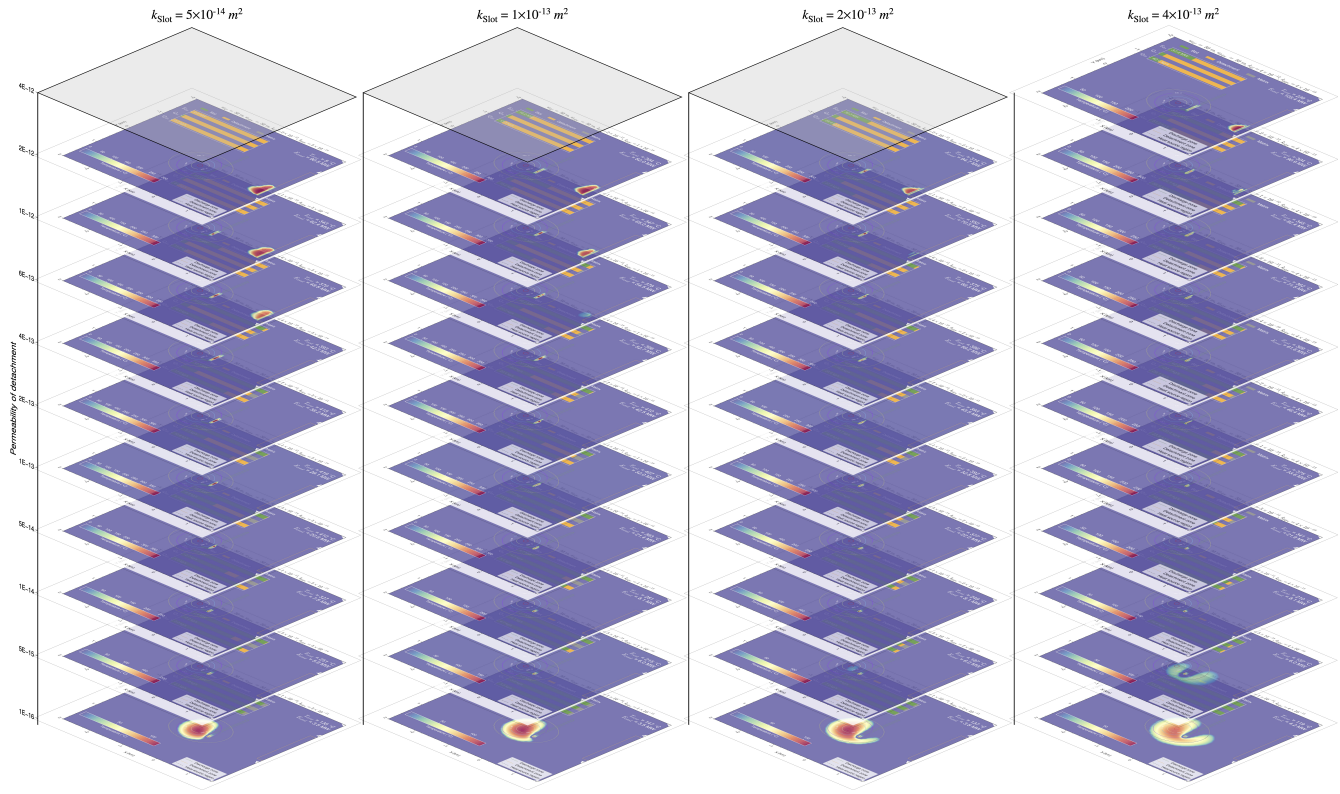

Supplementary Fig. 6: Summary of 3D model (slot geometry) results at quasi-steady state. Temperature field on seafloor, vent temperature T_{vent}, integrated total discharge mass flow rate Q_{dis} and heat output E_{dis}, conductive heat input E_{cond}

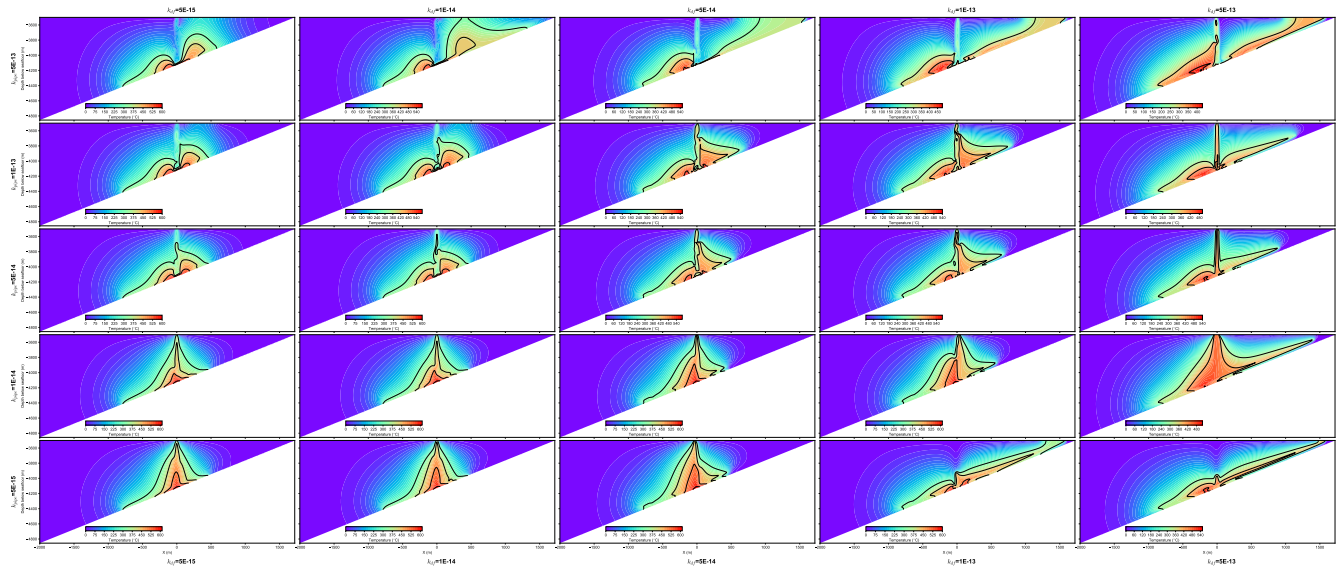

Supplementary Fig. 7: Temperature results of 2D models with presumed heat source on detachment. In this group of 2D models, the heat source temperature is 600 °C, width of detachment (w_{df}) and pipe (w_{pipe}) are 50 m and 100 m, respectively. Columns from left to right show results of models with different permeability of detachment fault (k_{df}) ranging from 5×10^{-15} m^2 to 5×10^{-13} m^2. Likewise, rows of subplots show results of models with different permeability of pipe (k_{pipe}) ranging from 5×10^{-15} m^2 to 5×10^{-13} m^2.

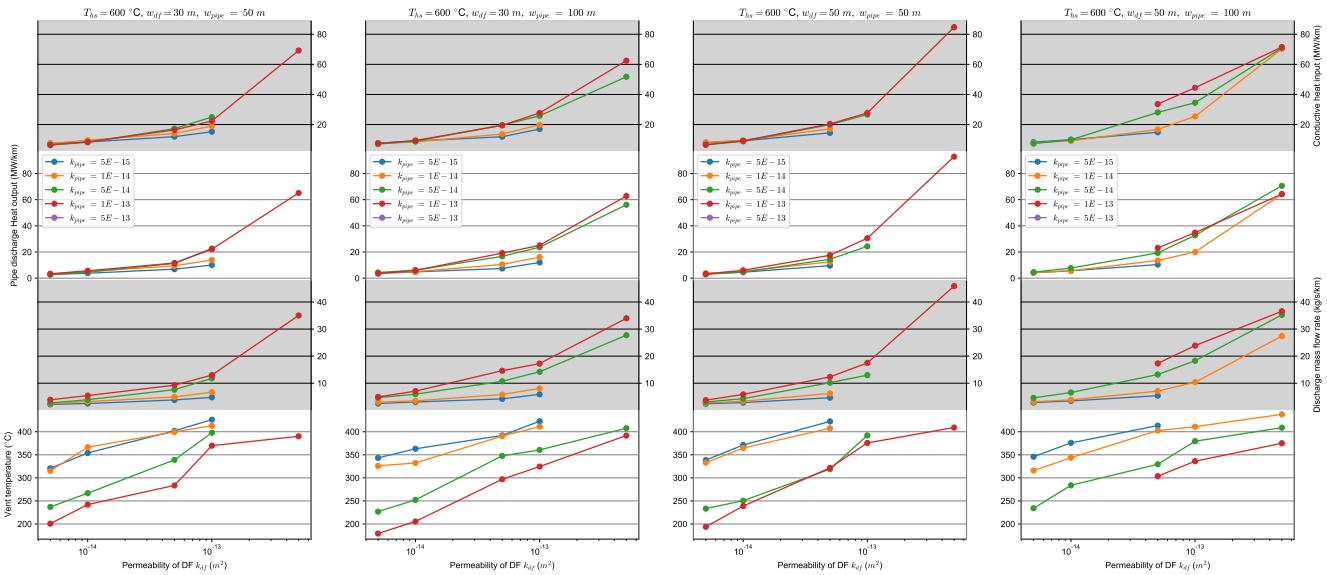

Supplementary Fig. 8: Summary of 2D model results. Rows of subplots from top to bottom show total conductive heat input (E_{cond}), total discharge heat output (E_{dis}), total discharge mass flow rate (Q_{dis}) and vent temperature, respectively. Columns of subplots from left to right show results of models with different width of detachment and pipe, the parameters are shown at the top side. As an example, the temperature field corresponding to the first column are shown in Supplementary Fig. 7. Note that model with some combination of parameters can not form an expected focused venting along pipe, for example $w_{df} = 30m, w_{pipe} = 50m$ (first column) and $k_{pipe} = 5 \times 10^{-14} m^2, k_{df} = 5 \times 10^{-13} m^2$. Result points of these kind of models are not shown in this figure.

S2. Supplementary Tables

References

[1] Fisher, A. T. Permeability within basaltic oceanic crust. *Rev. Geophys.* **36**, 143–182, DOI: 10.1029/97RG02916 (1998).

[2] Kopf, A. Permeability variation across an active low-angle detachment fault, western Woodlark Basin (ODP Leg 180), and its implication for fault activation. *Geol. Soc. London, Special Publ.* **186**, 23–41, DOI: 10.1144/GSL.SP.2001.186.01.03 (2001).

[3] Zhao, M., Canales, J. P. & Sohn, R. A. Three-dimensional seismic structure of a Mid-Atlantic Ridge segment characterized by active detachment faulting (Trans-Atlantic Geotraverse, 25°55′N-26°20′ N). *Geochem. Geophys. Geosystems* **13**, DOI: 10.1029/2012GC004454 (2012).

[4] Floyd, J., Mutter, J., Goodliffe, A. & Taylor, B. Evidence for fault weakness and fluid flow within an active low-angle normal fault. *Nature* **411**, 779–783, DOI: 10.1038/35081040 (2001).

[5] Pye, J. Freesteam project. https://sourceforge.net/projects/freesteam/ (2010).

[6] Guo, Z., Rüpke, L. & Tao, C. HydrothermalFoam v1. 0: a 3-D hydrothermal transport model for natural submarine hydrothermal systems. *Geosci. Model. Dev.* **13**, 6547–6565, DOI: 10.5194/gmd-13-6547-2020 (2020).

[7] Ludwig, R. J., Iturrino, G. J. & Rona, P. A. 23. Seismic velocity-porosity relationship of sulfide, sulfate, and basalt samples from the TAG hydrothermal mound. *Proc. Ocean. Drill. Program, Sci. Results; Tex. A & M Univ. Coll. Station. TX, USA* **158**, 313–328, DOI: 10.2973/odp.proc.sr.158.225.1998 (1998).

[8] Andersen, C., Rüpke, L., Hasenclever, J., Grevemeyer, I. & Petersen, S. Fault geometry and permeability contrast control vent temperatures at the Logatchev 1 hydrothermal field, Mid-Atlantic Ridge. *Geology* **43**, 51–54, DOI: 10.1130/G36113.1 (2015).

[9] Humphris, S. E. & Cann, J. R. Constraints on the energy and chemical balances of the modern TAG and ancient Cyprus seafloor sulfide deposits. *J. Geophys. Res. Solid Earth* **105**, 28477–28488, DOI: 10.1029/2000JB900289 (2000).

Table 1: List of parameters used in the equations and model result figures.

Symbol	Definition	Value	Unit
T	Temperature	-	°C
p	Pressure	-	Pa
$\vec{U}$	Fluid velocity	-	$m\ s^{-1}$
$\vec{g}$	Gravitational acceleration vector	9.8	$m\ s^{-2}$
k	Crustal permeability[1,2]	$10^{-16} - 10^{-11}$	m^2
k_{pipe}	Permeability of *pipe* shape of the permeable tectonic zone	-	m^2
k_{slot}	Permeability of *slot* shape of the permeable tectonic zone	-	m^2
k_{df}	Permeability of *detachment fault* zone	-	m^2
w_{df}	Thickness of detachment fault zone[3,4]	50 (30-200)	m^2
w_{pipe}	Diameter of pipe	100[❶]	m^2
T_{vent}	Maximum vent temperature	-	°C
Q_{dis}	Integrated total discharge mass flow rate	-	$kg\ s^{-1}$
Q_{re}	Integrated total recharge mass flow rate	-	$kg\ s^{-1}$
E_{dis}	Integrated total discharge heat output	-	MW
E_{cond}	Integrated total conductive heat power	-	MW
Fluid properties: calculated from IAPWS-IF97[5,6]			
ρ_f	Density	-	$kg\ m^{-3}$
μ_f	Dynamic viscosity	-	$Pa\ s$
C_{pf}	Specific heat	-	$J\ kg^{-1}\ K^{-1}$
H_f	Specific enthalpy	-	$J\ kg^{-1}$
H_0	Specific enthalpy of cold water	50,000	$J\ kg^{-1}$
α_f	Thermal expansivity	-	K^{-1}
β_f	Compressibility	-	Pa^{-1}
Rock properties: from reference[7,8]			
ε	Porosity	10	%
ρ_r	Density	2700	$kg\ m^{-3}$
C_{pr}	Specific heat	880	$J\ kg^{-1}\ K^{-1}$
λ_r	Thermal conductivity	2	$W\ m^{-1}\ K^{-1}$
Parameters for numerical modeling			
$\vec{S}_{face}$	Surface vector of cell face	$\|\|\vec{S}_{face}\|\|$	m^2
$\vec{S}_{patch}$	Surface vector of cell face on conductive boundary patch	$\|\|\vec{S}_{patch}\|\|$	m^2
Parameters used to estimate the volume of magma[9]			
L_H	Latent heat	6.8×10^5	$J\ kg^{-1}$
C_{pm}	Specific heat	1200	$J\ kg^{-1}\ K^{-1}$
ρ_m	Density	2800	$kg\ m^{-3}$

❶The diameter of the *pipe* in the 3D model is set to 100 m which is measuring from high-resolution bathymetry of TAG mound.